Low-frequency vibrational excitations in vitreous silica: the Ioffe-Regel limit

1999 J. Phys.: Condens. Matter 11 A219

(http://iopscience.iop.org/0953-8984/11/10A/018)

J. Phys.: Condens. Matter **11** (1999) A219–A227. Printed in the UK PII: S0953-8984(99)99630-3

Low-frequency vibrational excitations in vitreous silica: the Ioffe–Regel limit

S N Taraskin and S R Elliott

Department of Chemistry, University of Cambridge, Lensfield Road, Cambridge, CB2 1EW, UK

Received 2 October 1998

Abstract. The behaviour of vibrational plane waves in disordered solids has been studied theoretically, particularly in the vicinity of the Ioffe–Regel crossover. We have analysed the behaviour of vibrational excitations in vitreous silica, for which we have found the Ioffe–Regel crossover frequency to be $\nu_{IR} \simeq 1$ THz (for both longitudinal and transverse waves), in good agreement with experimental observations. Two methods have been used to obtain ν_{IR}: either by determining the decay time τ of the plane waves, or by analysing the distribution in $\boldsymbol{k}$-space of plane-wave components in the final scattered state of a plane wave.

1. Introduction

The influence of disorder in causing localization of waves propagating in disordered media continues to be much studied. Much work has been done in the past on localization of electrons [1], and there is current interest also in the localization of light in strongly scattering media [2]. However, perhaps one of the most fascinating areas of study in this regard concerns vibrational excitations in disordered materials.

One criterion that has been used in the past to signify the onset of localization is that of Ioffe and Regel [3]. As the degree of scattering of a wave increases, the mean free path, l, correspondingly decreases, and the Ioffe–Regel criterion is when the mean free path is comparable to the wavelength of the wave:

$$l_{IR} \simeq \lambda_{IR}. \tag{1}$$

In this circumstance, evidently a wave can no longer be readily defined. In the case of electrons, which are very strongly scattered by perturbations in electrostatic potentials associated, say, with structural disorder, simulations have shown that in fact the Ioffe–Regel criterion does correspond to the onset of electron localization [4]. For the case of vibrational excitations in disordered materials, the situation is not so clear cut [4, 5] because 'bare' localized vibrational states can become mixed (hybridized) with bare propagating phonon states; the resultant, resonant-like states are not spatially localized but instead are extended in character, albeit with their motion being diffusive, not propagating, in nature.

Recently, interest in the behaviour of vibrational excitations in the vicinity of the Ioffe–Regel crossover has been rekindled because of a number of inelastic neutron and x-ray scattering measurements carried out on v-SiO_2 [5, 7], the interpretation of which has been controversial [8].

In an attempt to shed additional light on this problem, we have undertaken a theoretical (that is numerical and analytic) study of the behaviour of plane-wave vibrational excitations

in vitreous (v-) SiO_2 in the vicinity of the Ioffe–Regel crossover. We have found thereby the first theoretical estimates for the values of parameters (frequency, wavevector) characterizing the crossover, and have established that phonon localization does *not* occur at the Ioffe–Regel crossover, nor are the vibrational excitations propagating in a simple sense above the crossover; instead they have a diffuse character [9, 10].

2. Model simulations

Models of v-SiO_2 have been constructed by N–P–T molecular-dynamics (MD) simulations, using a modified form [11] of the interatomic potential of van Beest *et al* [12]. All glassy models were created by quenching at an average rate of $\sim$1 K ps^{-1} from the melt at 6000 K, and the glassy state was subsequently relaxed to a well annealed state ($T \sim 10^{-4}$ K). Two types of model were constructed: a cubic model with $N = 1650$ atoms and a box length of $L \simeq 28.4$ Å, and a bar configuration containing $N = 1500$ atoms of size 85.6 Å $\times$ 15.6 Å $\times$ 15.6 Å allowing access to low values of wavevector ($k \gtrsim 0.07$ Å^{-1}) for vibrational modes propagating along the bar. In addition, several models of the crystalline polymorph, α-cristobalite, were constructed.

The fully dense dynamical matrices of the relaxed models were diagonalized directly, resulting in eigenvectors $\{\boldsymbol{e}^j\}$ and eigenvalues (frequencies) $\{\omega^j\}$ of the normal modes, allowing a complete harmonic vibrational analysis to be performed.

We have analysed the behaviour of vibrational excitations in the vicinity of the Ioffe–Regel crossover in two very different ways. The first makes use of equation (1) or, more precisely, the equivalent criterion:

$$\nu_{IR}\tau_{IR} \simeq 1 \tag{2}$$

where ν is the frequency of the vibrational wave, and τ is the decay time of the (plane) wave (since $l = c\tau$, where c is the wave velocity). The other treatment is in terms of an analysis of the wavevector components of the final state to which an initially plane wave is scattered by the disorder in the structure. Although the results in both cases have been obtained for the specific example of v-SiO_2, so that they can be compared with experimental data [5–7], nevertheless the methods are of general utility.

3. The Ioffe–Regel crossover: analysis of spectral densities

We have used two ways of estimating the decay time τ_k of the $\boldsymbol{k}$-component of an initially plane-wave vibrational excitation. The first is by determining the full width at half maximum (FWHM), Γ (measured in Hz) of the peaks in the spectral densities, since

$$\tau_k = 1/\pi\Gamma. \tag{3}$$

The spectral density, $|\alpha^j_{\boldsymbol{k}}|^2$, is related to the expansion coefficients involved in expanding an arbitrary vibrational excitation over eigenmodes, for example at time t:

$$\boldsymbol{u}(t) = \sum_{j=1}^{3N} \alpha^j_{\boldsymbol{k}} \frac{\boldsymbol{e}^j}{\sqrt{m}} \cos\omega^j t. \tag{4}$$

For the case of multicomponent systems, with atoms of differing masses (as in SiO_2), a number of closely related spectral densities can be defined, but they have very similar numerical values [13]. For reasons of simplicity, such relatively inessential details will be ignored henceforth.

For small values of $|\boldsymbol{k}| \ll 0.1$ Å^{-1}, well below the Ioffe–Regel limit and corresponding to the propagating phonon regime, the spectral densities are rather sharp peaks, more or less

symmetrical as a function of frequency, (although less so for the case of longitudinal modes). In such a case, the peaks can be fitted reasonably well by Lorentzian functions, the FWHM giving Γ and the peak position giving ν_k.

However, at larger values of $|\boldsymbol{k}| > 0.1$ Å^{-1}, the spectral-density peaks become increasingly asymmetric and indeed at mesoscopic values, $|\boldsymbol{k}| \simeq 1.0$ Å^{-1}, rather resemble the vibrational density of states (VDOS), a point to which we will return later. Such asymmetric peaks obviously cannot be fitted well by Lorentzians, and similar asymmetric peaks in the related dynamical structure factor measured by inelastic x-ray or neutron scattering have been fitted previously either by a damped harmonic oscillator (DHO) function [6] or by an empirical function [5], adapted from an analysis of the phonon–fracton crossover in aerogels. The use of the DHO function to fit the spectral density should not be used to infer any particular physical significance for the nature of the vibrational excitations beyond the Ioffe–Regel limit, since it can equally describe the damped behaviour of a localized oscillator or a propagating collective mode. Instead, it should be regarded simply as a suitable empirical function with which to fit asymmetric peaks.

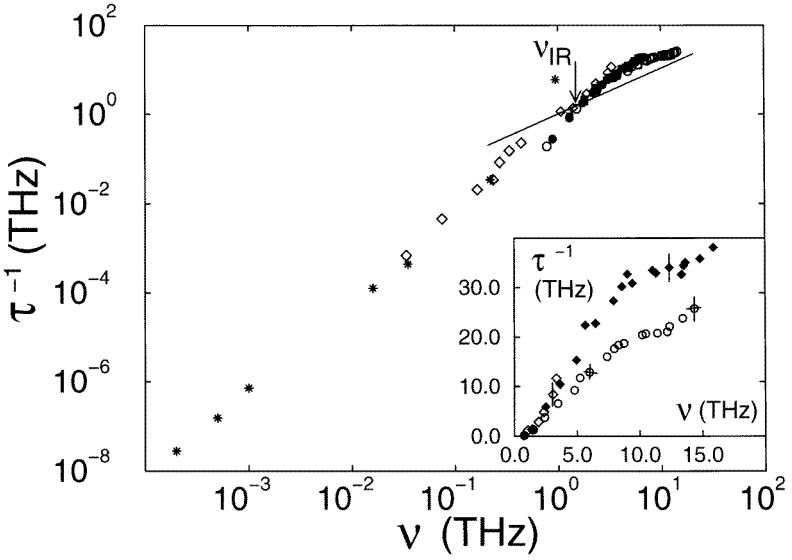

Figure 1. Inverse decay time versus average frequency of plane waves that are longitudinal (open circles and squares are for bar and cubic models) and transverse (solid circles and squares), together with experimental data (stars, [5]; open diamonds, [6]). The straight line is the function $\tau^{-1} = \nu$, and the crossover between the two curves marks the Ioffe–Regel limit. The values of τ^{-1} versus frequency of the initial plane wave given in the inset were obtained by a temporal-decay method (open circles) and from fits to spectral densities by the DHO model function (solid diamonds).

The spectral-density functions $|\alpha_k^j(\omega)|^2$ for the models of v-SiO_2 have been fitted by both Lorentzian and DHO functions to obtain values of τ_k, using equation (3), and the results are shown in figure 1. The intersection of the curve $\tau^{-1}(\nu)$ with the straight line $\tau^{-1} = \nu$ (cf equation (2)) defines the Ioffe–Regel crossover. For the case of our MD models of v-SiO_2, we find that $\nu_{IR} \simeq 1$ THz, *independent* of the polarization (longitudinal or transverse) of the initial plane wave. This theoretical estimate agrees very well with the value estimated from inelastic neutron scattering data for longitudinal excitations [5]. The corresponding crossover wavevectors are $k_{IR,t} \simeq 0.15$ Å^{-1} and $k_{IR,l} \simeq 0.1$ Å^{-1}.

The other way of estimating the decay time, τ_k, is by analysing directly the temporal decay of the wave amplitude. This has been done by fitting to the time-decaying quantity, $a_{k'}(t)$, that is the expansion coefficient involved in the expansion of a displacement vector, $\boldsymbol{u}(t)$, in plane waves,

$$\boldsymbol{u}(t) = \sum_{\boldsymbol{k}'} \boldsymbol{u}_{\boldsymbol{k}'}(t) \tag{5}$$

where

$$\boldsymbol{u}_{\boldsymbol{k}'}(t) = a_{k'}(t) A \hat{\boldsymbol{n}}' \cos(\boldsymbol{k}' \cdot \boldsymbol{r} + \phi_{k'}(t)) \tag{6}$$

and where A is a normalization constant and $\hat{\boldsymbol{n}}'$ is a unit polarization vector. The empirical function

$$f(t) = \exp(-t/\tau_k) |\cos(2\pi \bar{\nu}_k' t)| \tag{7}$$

has been used to fit the quantity $a_{\boldsymbol{k}}(t)/a_{\boldsymbol{k}}(0)$. The behaviour of $\tau_k(\bar{\nu})$ obtained in this way is very similar to that obtained from analysis of the spectral-density peak widths (see figure 1), yielding a very similar estimate for the Ioffe–Regel crossover frequency.

The crossover wavelength λ_{IR} or frequency ν_{IR}, given by equations (1) and (2), as originally proposed by Ioffe and Regel [3], do *not* correspond to the onset of complete vibrational localization, as has sometimes been suggested [5]. There is an indication of incipient localization at the frequency $\nu_{IR} \simeq 1$ THz, as evidenced by a marked dip in the value of the participation ratio for the vibrational modes [10], but we believe that only the 'bare', unreconstructed vibrational states (originating either from low-lying optic-like branches or high-k acoustic branches) become truly localized at the Ioffe–Regel limit. However, these states are mixed with bare propagating acoustic modes to give mixed, hybridized states that are not propagating but diffusive [14] in character.

The criteria given by equations (1) and (2) might be termed the first Ioffe–Regel crossover. A second limit is reached when, due to further increased strength of scattering, the mean free path reaches its minimum possible value, that is the average interatomic spacing, a, i.e.

$$l_{min} \simeq a. \tag{8}$$

This condition has been taken to signify the onset of localization of electrons in disordered materials [15], but that is not the case for vibrational excitations (at least for the case of v-SiO_2). Instead, this extreme strong-scattering limit corresponds to the incoherent limit, or the random-phase approximation, when the phase of the vibrational 'wave' fluctuates randomly from atomic site to site. In other words, this limit corresponds to the wavevector at which the spectral density can become broadened no further, i.e. when it starts to resemble the VDOS. This corresponds to an average frequency of $\bar{\nu}_k \simeq 5$ THz for v-SiO_2 and coincides with the point at which the curve of $\tau^{-1}(\nu)$ in figure 1 begins to turn over and flatten off. However, even this limit does not correspond to complete vibrational localization; this only occurs at the very extremities of the high-frequency bands in the VDOS for v-SiO_2, as revealed by the behaviour of the participation ratio [10].

4. The Ioffe–Regel crossover: analysis of the final scattered state

An initially plane vibrational excitation in a disordered material is scattered to a number of other plane waves having different wavevectors (and frequencies) because of the disorder and because a plane wave is not an eigenmode of the system. A signature of very strong scattering is that the variance (or uncertainty), Δk, in the wavevector of the final scattered plane waves is comparable to the wavevector of the initial state, i.e.

$$\Delta k \simeq k. \tag{9}$$

This strong-scattering criterion has also been taken [15] to be indicative of the Ioffe–Regel limit, marking the onset of localization (at least for electrons). We have made an analysis of the nature of the final scattered state of an initial plane vibrational wave in terms of the wavevector $\boldsymbol{k}'$ of the final state, and have proposed a new precise criterion for the Ioffe–Regel crossover somewhat related to equation (9). The analysis of the final state after scattering is, of course, complementary to the temporal-decay method described above and should give rise to similar conclusions and results.

Consider an initial plane-wave excitation, characterized by wavevector $\boldsymbol{k}$ and polarization $\hat{\boldsymbol{n}}$, scattered to a final state comprising different plane-wave components characterized by $\boldsymbol{k}'$ and $\hat{\boldsymbol{n}}'$. The quantity of interest is the distribution, $\rho(\boldsymbol{k}', \hat{n}'|\boldsymbol{k}, \hat{\boldsymbol{n}})$, of weights of different plane-wave components in the final state averaged over time. This can be written [13] as a sum over spectral densities, but the problem with using the spectral densities calculated from the vibrational eigenvectors for the relatively small models that we have studied is that the spectrum of modes in the particular region of interest, $\nu_{IR} \lesssim 1$ THz, is very sparse due to finite-size effects, and therefore the true behaviour of ρ is difficult to discern there. In order to circumvent this difficulty, we have calculated ρ using:

$$\rho(\boldsymbol{k}', \hat{\boldsymbol{n}}'|\boldsymbol{k}, \hat{\boldsymbol{n}}) = 3N \int_0^\infty g(\omega)|\alpha(\omega|k', \hat{n}')|^2|\alpha(\omega|k, \hat{n})|^2 \, \mathrm{d}\omega \tag{10}$$

where $g(\omega)$ is the VDOS. In the frequency region where the spectrum is sufficiently dense ($\nu \geqslant 0.6$ THz), we have used the VDOS and spectral densities calculated from the simulations. However, for lower frequencies, we have assumed that the VDOS can be approximated by the Debye law, and that the spectral densities can be represented as Lorentzians, whose peak positions are obtained from the dispersion law (using either calculated or experimental values of sound velocity) and widths obtained using an extrapolation of the quadratic frequency dependence found experimentally [5, 6] and in our simulations.

The results for ρ calculated in this way are shown in figure 2. It can be seen that, for very small values of wavevector (figures 2(a), (b)), an initial plane wave of either polarization type scatters to a final state consisting of *both* longitudinal {l} and transverse {t} polarizations, each having approximately the same frequency as the initial plane wave, $\nu' \simeq \nu$. Note that an initially {l} (or {t}) plane wave scatters to a (narrow) distribution of other {l} (or {t}) waves having the *same* average wavevector, but also to other {t} (or {l}) plane waves having greater (or smaller) wavevectors (since the sound velocities are such that $c_l > c_t$, and $\nu'_{l,t} \simeq \nu_{l,t}$).

As the wavevector of the initial plane wave increases, the widths $\delta k_{l,t}$ of the two peaks for the {l, t $\rightarrow$ l} and {l, t $\rightarrow$ t} channels increase (approximately quadratically with k, following the behaviour of $|\alpha^j_{\boldsymbol{k}}|^2$), as does the separation $\Delta k'$ of the two peaks in the ρ function (approximately linearly with k). In this picture, we ascribe the Ioffe–Regel limit to the condition when the two individual peaks for ρ_t and ρ_l merge to give a single peak in the total distribution function, $\rho_{tot} = 2\rho_t + \rho_l$, i.e. when

$$\Delta k' \simeq \delta k_{t,l}. \tag{11}$$

As seen from figures 2(c) and (d), this occurs at values of initial wavevector $k_l \simeq 0.1$ Å^{-1} and $k_t \simeq 0.15$ Å^{-1}, in agreement with the values inferred using the criterion $\nu_{IR}\tau_{IR} \simeq 1$ (figure 1). At yet larger values of initial wavevector, ρ_{tot} becomes a very broad and featureless asymmetric peak-shaped function. In this picture, therefore, the Ioffe–Regel crossover is associated with a transition from a weak-scattering regime ($\Delta k' \gg \delta k'$), where an initial plane wave is scattered to both longitudinal and transverse plane waves having roughly the same frequency and a narrow distribution of wavevectors, to a strong-scattering regime ($\Delta k' \ll \delta k'$), where the final scattered state consists of very many plane-wave components (both longitudinal and

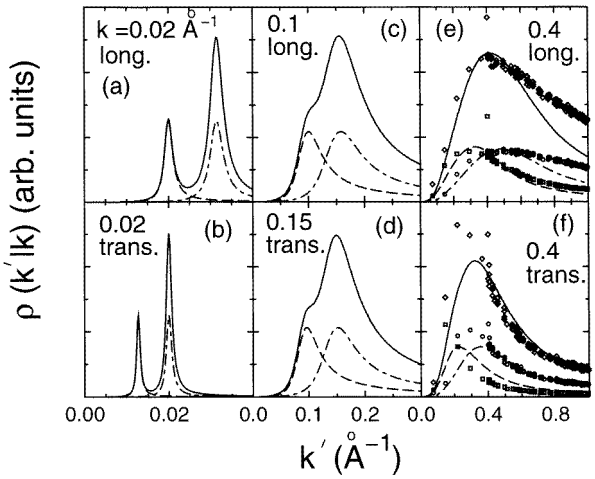

Figure 2. The distribution functions $\rho(\boldsymbol{k}', \hat{\boldsymbol{n}}_t'|\boldsymbol{k}, \hat{\boldsymbol{n}})$ (dot–dashed lines and circles), $\rho(\boldsymbol{k}', \hat{\boldsymbol{n}}_l'|\boldsymbol{k}, \hat{\boldsymbol{n}})$ (dashed lines and squares) and $\rho_{tot}(\boldsymbol{k}'|\boldsymbol{k}, \hat{\boldsymbol{n}})$ (solid lines and diamonds) for longitudinal, (a), (c), (e), and transverse, (b), (d), (f) initial polarizations of plane waves characterized by different initial wavevector magnitudes. Plots (c) and (d) correspond to the Ioffe–Regel crossover. The lines represent the results for an analytical model while the symbols are from numerical simulations.

transverse), characterized by wavevector magnitudes differing from the initial one by values of the order of the initial $\boldsymbol{k}$ magnitude itself.

5. Discussion

As follows from equation (10), plane waves scatter not only to modes of approximately the same wavelength but also to modes of rather different wavelength but of similar frequency. We have confirmed this conclusion by numerical analysis at not very low wavevectors (see the symbols in figures 2(e) and (f)). Such an effect is due to structural disorder, causing the coupling of plane waves with different wavevectors and polarizations but similar energies. A possible scenario explaining such coupling is based on the following qualitative picture of the vibrational spectrum of disordered structures.

We suppose [10] that the vibrational states in the low-frequency region comprise two sets of bare states, plane waves (Debye spectrum) and band-tail states, which are mixed together. The bare band-tail states can originate, for example, from a low-lying optic band in the crystalline counterpart, and/or from the short-wavelength part of the acoustic band. The structural disorder destroys the band-like spectrum of the crystalline counterparts and pushes the states up and down in frequency, leading to the appearance of band tails. The bare localized states from the lowest tail interact with acoustic waves because they lie in the same frequency range. Coupling coefficients are hardly sensitive to the polarization of acoustic waves so that the resulting resonant states (eigenmodes) roughly equally contain plane waves of different polarizations (different wavevectors) and approximately of the same frequency.

Such a very qualitative picture can be supported by the results of our numerical simulations for v-SiO_2, where around $\nu \simeq 1$ THz we indeed found resonant-like states containing both localized and wave-like constituents (see figure 3(a)). In figure 3(a) we show a real-space representation of the eigenmode having frequency $\nu \simeq 1.05$ THz and characterized by the

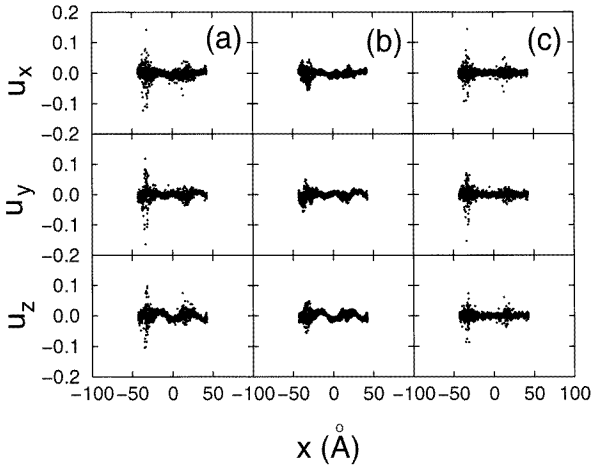

Figure 3. (a) Real-space representation of the atomic displacements projected along the bar direction (x) for an eigenmode with frequency $\nu \simeq 1.05$ THz and participation ratio $p \simeq 0.08$. (b) Acoustic-like plane-wave contributions with a wavevector cutoff $k^* = 0.8$ Å^{-1}. (c) Difference between (a) and (b), showing the localized components (large amplitude) and the 'random' constituent.

participation ratio, $p \simeq 0.08$. As clearly seen from figure 3(a), this eigenmode contains both localized and non-localized (wave-like) components. The major part of the wave-like component is represented by a mixture of longitudinal waves having wavelengths equal to half the box size, $\lambda = L_x/2$, and transverse waves with wavelength, $\lambda = L_x/3$ (figure 3(b)). The localized component is characterized by large atomic displacements (mainly of oxygen atoms) and contains two localized contributions separated in space (a pronounced one around $x \simeq -40$ Å and a less pronounced one around $x \simeq 20$ Å).

In order to understand the origin of the localized component, we extracted it from the eigenmode in the following manner. First, we expanded the eigenmode in plane waves with all polarizations and calculated the distribution of the weights of different plane waves. Such a distribution is combined from two distributions of the weights of longitudinal and transverse waves, which are peak-shaped with the peak position around $k_{t,l} \simeq 2\pi\nu/c_{t,l}$ [16]. Then we removed the major acoustic component (see figure 3(b)) from the eigenmode by subtracting all plane waves having wavevectors in the peak regions of the distributions of the weights. In practice, we removed from the eigenmode all plane waves having wavevector magnitudes less than a certain cutoff, k^*. The value k^* has been chosen so that varying it does not change significantly the shape of the rest of the eigenmode (e.g. $k^* = 0.8$ Å^{-1}). After removing the acoustic component, we found the rest of the eigenmode to be comprised of the localized part and a so-called random component [17] (see figure 3(c)). The random component can be imagined as a short-wavelength part in the Fourier expansion of the eigenmode. It should be noted that by considering only a set of plane waves propagating along the bar, the shape, but not the width, of the 'acoustic-like' component of the eigenmode can be reproduced. However, the width of the acoustic-like component becomes comparable to that of the eigenmode when plane waves propagating in *different* directions are included. However, subtracting this component from the total eigenmode gives a 'random' component still of comparable width to the acoustic-like component. It may be that the random component is simply an artifact of the finite size of the simulation box: were more waves propagating in yet more directions to be included, it is

plausible that the entire non-localized part of the eigenmode could be represented as a sum of a number of plane waves. The displacements of atoms in the random component, $\langle u_{ran}\rangle$, are much smaller than those in the localized one, $\langle u_{loc}\rangle$. Therefore we are able approximately to separate the localized component (with accuracy $\langle u_{ran}\rangle/\langle u_{loc}\rangle$) by choosing atoms having displacements larger than a certain cutoff ($u > u^*$, e.g. with $u^* = 0.1$). The resulting localized constituent (located at around $x \simeq -40$ Å) is shown in figure 4. The motion of atoms for such a localized bare vibration can be imagined as coupled displacements and rotations of SiO_4 tetrahedra (see figure 4). We have compared these vibrations with the short-wavelength vibrational motions in α-cristobalite of similar frequency and found them to be very similar to each other.

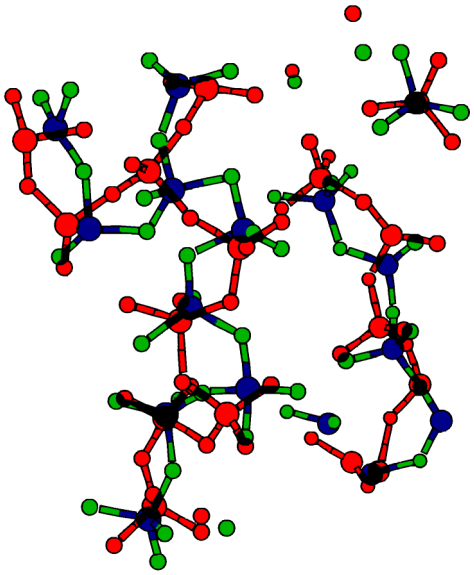

Figure 4. Real-space visualization of the atomic motions characterizing the localized constituent of the eigenmode at $\nu \simeq 1.05$ THz (localized at $x \simeq -40$ Å in figure 3). The figure is a superposition of two snapshots of the mode at different times: in one snapshot, silicon atoms are coloured blue and oxygens are green, and in the other silicons are orange and oxygens are red. The localized mode has been extracted from the resultant displacement pattern shown in figure 3(c) by considering only those atoms (16 oxygens and two silicons) having displacements greater than $u^* = 0.1$. The nearest-neighbour atoms to these atoms with greatest displacement have also been included for ease of visualization. The motion consists of rotational and translational displacements of coupled SiO_4 tetrahedra.

We would like to stress that in macroscopic systems the bare localized components in the low-frequency regime are actually dispersed in the dense acoustic spectrum. Only due to the finite size of the simulation box and, as consequence of this, a not very dense acoustic spectrum, are we able to distinguish the bare localized component and investigate it.

6. Conclusions

We have investigated theoretically the Ioffe–Regel limit for vibrational excitations in vitreous SiO_2 using structural models constructed using molecular dynamics. We find the Ioffe–Regel crossover frequency to be $\nu_{IR} \simeq 1$ THz for both longitudinal and transverse plane-wave excitations, with corresponding crossover wavevectors $k_{IR,l} \simeq 0.1$ Å^{-1} and $k_{IR,t} \simeq 0.15$ Å^{-1}.

Consistent theoretical estimates have been obtained using very different methods, involving either the decay time of plane waves (evaluated in several ways), or the distribution of wavevectors of plane-wave contributions characterizing the final scattered state. Although these methods have been applied to the particular case of glassy silica, for which relevant experimental data are available, nevertheless the methods are completely general.

Acknowledgments

The financial support of the Engineering and Physical Sciences Research Council, and Trinity College and the Newton Trust, Cambridge, is gratefully acknowledged.

References

[1] Kamimura H and Aoki H 1989 *The Physics of Interacting Electrons in Disordered Systems* (Oxford: Clarendon)
[2] Wiersma D S, Bartolini P, Lagendijk A and Righini R 1997 *Nature* **390** 671
[3] Ioffe A F and Regel A R 1960 *Prog. Semicond.* **4** 237
[4] Sheng P, Zhou M and Zhang Z-Q 1994 *Phys. Rev. Lett.* **72** 234
[5] Foret M, Courtens E, Vacher R and Suck J-B 1996 *Phys. Rev. Lett.* **77** 3831
[6] Benassi P, Krisch M, Masciovecchio C, Mazzacurati V, Monako G, Ruocco G, Sette F and Verbeni R 1996 *Phys. Rev. Lett.* **77** 3835
[7] Wischnewski A, Buchenau U, Dianoux A J, Kamitakahara W A and Zarestky J L 1998 *Phys. Rev. Lett.* **57** 2663
[8] See for example the comments by Foret M, Courtens E, Vacher R and Suck J-B 1997 *Phys. Rev. Lett.* **78** 4669
Benassi P, Krisch M, Masciovecchio C, Mazzacurati V, Monako G, Ruocco G, Sette F and Verbeni R 1997 *Phys. Rev. Lett.* **78** 4670
[9] Taraskin S N and Elliott S R 1997 *Europhys. Lett.* **39** 37
[10] Taraskin S N and Elliott S R 1997 *Phys. Rev.* B **56** 8605
[11] Guissani Y and Guillot B 1995 *J. Chem. Phys.* **104** 7633
[12] van Beest B W H, Kramer G J and van Santen R A 1990 *Phys. Rev. Lett.* **64** 1955
[13] Taraskin S N and Elliott S R to be published
[14] Fabian J and Allen P B 1996 *Phys. Rev. Lett.* **77** 3839
[15] Mott N F and Davis E A 1979 *Electronic Processes in Non-Crystalline Materials* 2nd edn (Oxford: Clarendon)
[16] Taraskin S N and Elliott S R 1998 *Phil. Mag.* B **77** 403
[17] Montagna M, Ruocco G, Viliani G, Di Leonardo R, Dusi R, Monaco G, Sampoli M and Scopigno T *Preprint*